Published in final edited form as:
Neurogastroenterol Motil. 2009 July ; 21(7): 778–e50. doi:10.1111/j.1365-2982.2009.01265.x.

Biomagnetic signatures of uncoupled gastric musculature

L. A. Bradshaw[*,†,‡], **A. Irimia**[§], **J. A. Sims**[¶], and **W. O. Richards**[*]

[*]Department of Surgery, Vanderbilt University Medical Center, Nashville, TN, USA

[†]Department of Physics & Astronomy, Vanderbilt University, Nashville, TN, USA

[‡]Department of Physics, Lipscomb University, Nashville, TN, USA

[§]Department of Radiology, University of California, San Diego, CA, USA

[¶]Department of Biomedical Engineering, University of North Carolina, Chapel Hill, NC, USA

Abstract

Gastric slow waves propagate in the electrical syncytium of the healthy stomach, being generated at a rate of approximately three times per minute in a pacemaker region along the greater curvature of the antrum and propagating distally towards the pylorus. Disease states are known to alter the normal gastric slow wave. Recent studies have suggested the use of biomagnetic techniques for assessing parameters of the gastric slow wave that have potential diagnostic significance. We present a study in which the gastric syncytium was uncoupled by mechanical division as we recorded serosal electric potentials along with multichannel biomagnetic signals and cutaneous potentials. By computing the surface current density (SCD) from multichannel biomagnetic recordings, we were able to quantify gastric slow wave propagation as well as the frequency and amplitude of the slow wave and to show that these correlate well with similar parameters from serosal electrodes. We found the dominant slow wave frequency to be an unreliable indicator of gastric uncoupling as uncoupling results in the appearance of multiple slow wave sources at various frequencies in external recordings. The percentage of power distributed in specific frequency ranges exhibited significant postdivision changes. Propagation velocity determined from SCD maps was a weak indicator of uncoupling in this work; we believe that the relatively low spatial resolution of our 19-channel biomagnetometer confounds the characterization of spatial variations in slow wave propagation velocities. Nonetheless, the biomagnetic technique represents a non-invasive method for accurate determination of clinically significant parameters of the gastric slow wave.

Keywords

electrogastrography; gastric slow wave; magnetogastrography; SQUID magnetometer

Introduction

The slow wave of the stomach—also known as the electrical control activity or basic electrical rhythm—originates in the interstitial cells of Cajal (ICCs) along the greater curvature of the antrum. Populations of ICCs and smooth muscle cells are electrically coupled and thus isopotential, exhibiting a depolarization/repolarization cycle that repeats about every 20 s in humans. Interstitial cells of Cajal propagate the slow wave quickly in a

Address for correspondence: Leonard A. Bradshaw, Box 1807 Station B, Department of Surgery, Vanderbilt University, Nashville, TN 37235, USA., Tel: 615 322 2828; fax: 615 322 4977; alan.bradshaw@vanderbilt.edu, alan.bradshaw@lipscomb.edu.

circumferential direction around the body of the stomach. The slow wave then propagates more slowly down the stomach's longitudinal axis from the pacemaker location in the antrum to the pylorus, where the gastric slow wave terminates. However, the specific propagation route is highly complex and not uniform, potentially even stepwise.[1,2]

Several authors have suggested that, although potentially challenging, non-invasive measurements of slow wave parameters such as amplitude, frequency and propagation velocity could have diagnostic value.[3–6] Although intervening tissue layers distort and attenuate the electric potential from the slow wave, cutaneous electrodes are sometimes capable of recording the electrogastrogram (EGG). The cutaneous potential thus reflects the frequency of the underlying slow wave reliably,[7] but there is a complex relationship between slow wave and EGG amplitudes.[8–12] Nonetheless, the absence of a postprandial EGG amplitude increase may have diagnostic significance.[3,13,14] Recent studies have suggested that the EGG may reflect propagation characteristics,[15] but reliable determination of propagation velocities from EGG recordings has not been demonstrated. Additionally, even the putative clinical utility of frequency dynamics in EGG has been questioned on the basis of low reproducibility.[16]

Uncoupling of the gastric musculature affects the gastric slow wave. Mintchev *et al.* showed that spectral analysis of the EGG could recognize severe gastric uncoupling,[17] while Liang and Chen suggested that gastric uncoupling could cause a decrease in the amplitude of the EGG.[18] However, there has been a great deal of controversy regarding the utility of EGG amplitude measurements because they depend strongly on a number of different important factors, including the separation between the stomach and skin[19] as well as the conductivity of abdominal fat layers.[20] Won *et al.* recently showed that changes in slow wave frequency induced by stretch of the antral musculature caused gastric uncoupling that inhibited propagation.[21]

The magnetogastrogram (MGG) measures the same underlying electrical activity as the EGG.[22–26] Superconducting quantum interference device (SQUID) magnetometers have unrivalled sensitivity for detecting the weak magnetic fields associated with the slow wave (fields on the order of picotesla, pT). Multiple biomagnetic sensors facilitate straightforward multichannel spatiotemporal sampling that allows evaluation of gastric slow wave frequency, amplitude and propagation velocity.[25] Our aim in this study was to determine whether non-invasive biomagnetic measurements from a SQUID magnetometer could identify gastric uncoupling.

Materials and Methods

Nine adult pigs were anaesthetized by induction with ketamine/xylazine/telazol (2.2/2.2/4.4 mg kg^{-1}) i.m. and maintained with isoflurane (1.5–3.0 % with O_2) to provide a steady plane of anaesthesia throughout the study according to a protocol approved by the Vanderbilt University Institutional Animal Care and Use Committee. Animals were also maintained on a ventilator throughout the experiment. We performed a laparotomy and attached bipolar electrode platforms to the antrum of the gastric serosa proximal and distal to a transverse line used to divide the stomach surgically. Electrode platforms consisted of three rows of four bipolar electrode pairs each, with the four electrodes oriented along the gastric longitudinal axis so as to allow measurement of gastric slow wave propagation. The laparotomy was closed and three cutaneous electrodes were placed in the epigastric region along the same line as the serosal electrodes to measure the EGG. The animal was placed underneath the Tristan 637i (Tristan Technologies, San Diego, CA, USA) biomagnetometer in a magnetically shielded room. Respiration was suspended periodically to provide periods of reduced motion.

Our biomagnetometer consists of a collection of SQUID gradiometers (5.0 cm baseline) that record data at 29 sensor locations using an array of detection coils. The detection coils are located in a plane at the bottom of a dewar filled with liquid helium (temperature ~4 K) and are inductively coupled to SQUID sensors that convert magnetic flux threading the detection coils to voltage signals.[27] The voltage data were amplified and collected on a PC (Dell Computer, Austin, TX, USA) running LabVIEW (National Instruments, Austin, TX, USA). Ten of these sensors are oriented tangential to the bottom of the dewar, and for this study, we utilized only the data from the 19 sensors oriented normal to the dewar bottom, arranged in a hexagonal close-packed spacing. The approximate location of the SQUID magnetometer relative to the position of the stomach and the serosal electrodes as well as the location of the gastric division are illustrated in Fig. 1.

We first measured simultaneous MGG, serosal electromyogram (EMG) and cutaneous EGG signals for a 30 min baseline. After the baseline recording, the stomach was surgically divided between the proximal and distal antrum. Simultaneous recording was continued for a period of 1 h following gastric division.

We used MATLAB (MathWorks, Natick MA) to analyse data postacquisition. The general analysis procedure involved pre- and post-filtering the data using a second-order, zero-phase Butterworth filter with a bandpass of 1–100 cycles per minute (cpm). The zero-phase nature of the filter allows us to accurately analyse signals in the spatiotemporal domain for assessment of gastric propagation. We performed spectral analysis on the signals using autoregressive (AR) spectral analysis.[28] The spectra were further analysed to determine the frequency of the dominant peaks, as well as frequencies of other significant spectral peaks. In addition, we determined the percentage of power distributed (PPD) in the spectra in frequency ranges defined as bradygastric (lower than two standard deviations from the mean gastric frequency determined by serosal electrode recordings) and tachygastric (higher than two standard deviations from the mean gastric frequency).

Filtered biomagnetic data were also subjected to surface current density mapping in order to assess propagation.[29] The surface current density (SCD) provides a measure of the spatial differences in the magnetic field that would be associated with currents flowing just underneath the surface of a volume conducting body.[30] Although they do not represent a physiological current density in our experimental subjects, the SCD is a useful tool for visualizing the likely spatiotemporal patterns of bioelectric current that could produce the measured magnetic field data.[30] Maxima of SCD maps tracked over time give an estimate of the propagation velocity of the gastric slow wave. This velocity is estimated by a linear fit to the maximum location as a function of time, allowing us to estimate the propagation velocity as the slope of the best-fit line.

Independent component analysis is a blind signal separation (BSS) method for multivariate data that has been widely applied to physiological measurements. A detailed description of independent component analysis (ICA) and of its mathematical underpinnings is available in,[31] where we showed that independent components (ICs) more closely reflect underlying temporal frequency information from biomagnetic sources. For this reason, data were also subjected to ICA, which helped us to separate data of gastric and non-gastric origin. ICA components were further analysed and compared with data from conventional filtering.

Results

Gastric slow waves were recorded from serosal electrodes as well as from the SQUID. In electrode data sets from the distal antrum, apparent spiking activity (also known as electrical response activity) superimposed on the slow wave complicated the identification of slow

waves in the raw data. However, slow waves could be identified in filtered electrode data. Fig. 2 shows typical serosal electrode recordings that are both unfiltered (i) and filtered (ii). In three of the nine studies, no periodic spiking activity was present, but serosal potentials and transabdominal magnetic fields from those studies still show clear slow waves.

Artefacts from respiratory and cardiac magnetic interference required us to filter magnetic data. As a result, we did not observe spiking activity reflected in the filtered magnetic signal from these data, although we have seen such activity in previous studies.[32,33] Fig. 2Aiii, Biii show MGG signals corresponding to the serosal potentials shown in Fig. 2Ai, Bi, respectively, mapped to the locations of the SQUID sensors. During breathholds—in which both slow waves and spikes were observed in serosal electrodes—only slow waves were noticeable in magnetic data, suggesting that SQUID signals primarily reflect the gastric slow wave, although it is possible that filtering to remove cardiac interference also removed the signature of spiking activity from the MGG data.

Fig. 3 shows a simultaneous recording of MGG, serosal EMG and EGG with the associated AR power spectra, and the MGGs from each subject are displayed with their associated power spectra in Fig. 4. The power spectra allow identification of dominant signal frequencies. At baseline, the SQUID magnetometer recorded slow waves with the same frequencies of 2.8 ± 0.2 cpm (mean ± standard error of the mean, SEM) as recorded by serosal electrodes (proximal: 3.1 ± 0.1 cpm, $P = 0.12$; distal: 3.0 ± 0.1 cpm, $P = 0.23$). Electrogastrogram frequencies were slightly decreased but were not significantly lower (2.6 ± 0.2 cpm, $P = 0.06$). Signal amplitudes were difficult to estimate because of noise contributions from respiration, cardiac and motion. During respiration suspension with cardiac activity filtered, the slow wave amplitude in the healthy state was found to be 1.6 ± 0.5 mV (mean ± SEM) in serosal electrodes, 4.2 ± 0.9 pT in the MGG and 200 ± 62 μV for EGG. There was a slight, but not statistically significant, decrease in the amplitudes postdivision for all modalities (1.1 ± 0.4 mV serosal, 2.9 ± 0.8 pT MGG, 162 ± 42 μV EGG).

The slow wave propagated with a velocity between 4.5 and 6.0 mm s^{-1} as measured by visual inspection of phase shifts in sequential distal serosal electrodes. Signals from the more proximal electrode platform did not consistently exhibit regular propagating slow waves that would allow computation of phase shifts or of propagation velocity. Phase shifts were also not observed consistently in either EGG or MGG recordings, but SCD mapping of the MGG signals allowed us to identify a propagation velocity of 5.3 ± 0.5 mm s^{-1}, similar to that seen in serosal electrodes. Consecutive SCD maps before and after division in a typical subject are shown in Fig. 5. From these maps, we computed the location of the pattern maximum as a function of time to estimate the propagation velocity as shown the bottom of Fig. 5. The estimated velocity is the slope of the best-fit line to the pattern maximum data.

After division of the stomach, slow waves evaluated by standard filtering methods in both proximal serosal electrode data and in SQUID data showed no significant change in dominant frequency (proximal EMG: 3.1 ± 0.2 cpm, $P = 0.43$; MGG: 3.0 ± 0.4 cpm, $P = 0.37$; Fig. 6A). The serosal electrodes distal to the division, however, did show a significant decrease in dominant frequency (2.2 ± 0.3 cpm, $P < 0.01$) We noted a much larger variance in postdivision frequencies from both electrodes and the SQUID, indicating that more diverse dominant slow wave frequencies were recorded postdivision which, on average, did not differ significantly from predivision values. As illustrated in Fig. 3D–F, a typical postdivision power spectrum contains multiple peaks that tend to complicate the identification of a particular peak as ‘the’ dominant gastric slow wave frequency. We observed a significant increase in the number of peaks in MGG power spectra after gastric

division, which was not seen in either proximal or distal serosal electrodes (Fig. 6B). This increase indicates that while slow waves in particular regions of the gastric syncytium may exhibit different specific dominant frequencies, magnetic fields from multiple regions are detected by the SQUID. The presence of multiple peaks in the power spectrum is an indication of gastric uncoupling. The EGG data did not exhibit a significant change in dominant frequency (2.7 ± 0.3 cpm, $P = 0.34$) or number of spectral peaks.

Independent component analysis revealed components of the data that exhibited a substantial postdivision frequency decrease from baseline values of 2.91 ± 0.47 cpm (serosal) and 3.09 ± 0.91 cpm (MGG) to postdivision frequencies of 1.22 ± 1.04 cpm (serosal) and 1.38 ± 1.17 cpm (MGG). The larger standard deviation indicates the wider postdivision range of dominant frequencies characteristic of uncoupled tissue.

The percentage of power distributed in bradygastric frequencies was significantly increased after gastric division in both serosal electrode and MGG data, as seen in Table 1. The only other statistically significant difference in pre and postdivision PPDs was a decrease in normogastric power noted in serosal electrodes. The decrease in normogastric power for MGG was not statistically significant. There was no significant change in power at tachygastric frequencies in any modality. No effect was observed in EGG PPDs.

Comparison of SCD maps with serosal electrode signals showed similar predivision slow wave propagation patterns. The propagation velocity could be estimated by computing the location of the SCD maxima at successive time intervals and then determining the ratio of change in position of the maximum to the elapsed time. Because of the relatively low spatial resolution of the SQUID magnetometer used in this study, we found it most reliable to estimate propagation velocity over the extent of the propagation pattern by linear correlation. Although a spatial velocity gradient could be estimated using this technique, there is a concomitant decrease in the accuracy of the estimation. Additionally, as only our distal antral electrodes reliably recorded slow waves, we did not observe a significant spatial difference in EMG propagation velocities. The propagation velocities determined from distal antral serosal electrodes are summarized in Table 2 along with the propagation velocity estimated from SCD maps computed from MGG recordings. After gastric division, although there was more variance in the propagation velocity recorded from more distal antral serosal electrodes, no significant difference in the mean propagation velocity was determined. The MGG SCD propagation velocity also exhibited a substantial increase in variance, but there was also a weakly significant postdivision velocity decrease ($P = 0.05$).

Discussion

We evaluated signals recorded from the multichannel MGG simultaneous with multiple serosal potential measurements (EMGs) and EGGs in porcine subjects before and after gastric division. Our results show that the MGG reflects the underlying slow wave activity of the stomach. Similar baseline frequencies were recorded in all modalities.

Gastric division causes the development of ectopic pacemakers that continue to drive slow wave activity, but at lower frequencies. However, other regions of the gastric syncytium not covered by our local electrode array are driven by pacemakers at still different frequencies. Thus, although we did not observe a concomitant decrease in MGG slow wave dominant frequency, we did observe an increase in the number of peaks in postdivision power spectra. The MGG records gastric slow waves from multiple uncoupled regions of the stomach. We were able to distinguish these contributions using ICA, and analysis of the components determined from ICA showed a significant postdivision frequency decrease.

We observed significant increases in the percentage of power distributed in frequencies below the normal gastric range in serosal electrode and MGG recordings, which suggests that ectopic slow waves are indeed detected by MGG. The cutaneous EGG showed a statistically insignificant increase in power contained in bradygastric frequencies. Previous studies by Mintchev *et al.* have suggested that EGG is capable of detecting uncoupling in canine subjects using spectral analysis and measures of chaos,[17,34] while Irimia and Wikswo also used chaos measures to characterize abnormal gastric slow waves.[35] It is likely that the additional abdominal fat in the porcine model complicated the accurate reflection of slow waves in the cutaneous electrodes. Also, it was not possible for us to apply the same detection criteria used in the Mintchev study because of our requirement of respiration-free data segments.

We have begun utilizing data processing methods for rejection of noise artefacts in the data that could significantly improve our ability to use longer time segments in our analyses and provide a more robust comparison with other studies. However, many of these techniques compromise spatial information contained in the data to highlight temporal signal features and thus, their utility for assessing propagation is questionable. Nonetheless, we expect such techniques to provide for more accurate temporal analyses. One of the primary noise components to our signal was caused by respiration, which was suspended periodically during the course of our studies. Irimia previously showed that ICA is a very effective technique for reducing respiratory interference in biomagnetic signals from the GI tract.[36] As in that study, we were able to isolate data of gastric origin from other data in terms of the frequency content; nevertheless, it can be a difficult task to determine which independent components warrant inclusion in a particular analysis, and the development of specific criteria is still underway.

The multichannel MGG measurements allowed us to compute a gastric slow wave propagation velocity from the computed surface current density maps that agreed with the velocity obtained from antral serosal electrodes. The serosal recordings were somewhat noisier than might be expected, particularly when compared with the monopolar *ex vivo* recordings made by Lammers *et al.*[37] or microelectrode recordings such as those reported by Bauer *et al.*[38] Nonetheless, the propagation velocities we obtained are in good agreement with those previously reported from other labs.[38] Our bipolar electrode arrangement was designed primarily to help reduce motion artefact which contributes significantly to our *in situ* data. Gastric uncoupling was associated with an increase in the variance of propagation velocities determined from SCD maps. Cutaneous EGG did not contain phase differences that would allow computation of propagation velocities. While we did observe propagation in both distal serosal electrodes and postdivision SCD maps, it was substantially more variable than before division. The presence of multiple frequencies recorded in the SQUID are strongly suggestive of ectopic pacemakers that would inhibit propagation, and could thus cast doubt on the validity of postdivision propagation velocity estimates. The distal serosal electrode platform did not exhibit the same multiple frequencies or indications of uncoupling as the SQUID, and we did observe postdivision slow wave propagation in serosal electrodes. It is possible that the serosal electrodes record locally consistent propagating activity while the SQUID additionally detects multiple frequencies characteristic of an uncoupled gastric syncytium.

The spatial resolution of our Tristan 637i biomagnetometer did not facilitate a characterization of spatial gradients in slow wave propagation velocity with SCD maps. The spatial separation of our sensors is approximately 4 cm. While we were able to position the magnetometer in the optimal location for detection of gastric propagation, an improper location of the biomagnetometer distant from the gastric musculature would reduce the spatial resolution even further. We determined propagation velocity as the slope of the best-

fit line to the SCD pattern maxima as a function of time to obtain a single propagation velocity estimate for the entire gastric slow wave propagation, though it is well known that propagation velocity is non-uniform and increases in the aborad direction.[39,40] We could have used a higher-order polynomial fit or a linear fit to shorter data segments, but these tended to produce a mix of accurate and obviously inaccurate propagation velocities with our relatively low spatial resolution. A more densely packed array of SQUID detectors would greatly enhance the capability to determine propagation velocity from slow waves in different parts of the gastric musculature, and we intend to pursue these methods in future studies.

Chen *et al.* were able to identify phase shifts in a four-channel cutaneous EGG setup.[15] Our recording setup limited the number of EGG channels to three in this experiment, which is one potential explanation for our inability to detect consistent phase shifts in the EGG. Also, the ability to detect phase shifts is dependent on the thickness of the abdomen, and so our measurements in porcine subjects may not be directly comparable to the human studies of Chen *et al.* Additionally, their method does not allow computation of the propagation velocity. It is significant to note that we were able to identify gastric uncoupling using MGG with a single division, whereas in Mintchev's previous study, EGG was only able to recognize severe gastric uncoupling from multiple gastric divisions.[17] These data suggest that MGG may be a more sensitive indicator of the underlying electrophysiology.

It is also possible that laparotomy itself has some effect on the cutaneous EGG as it necessarily changes the electrical continuity of the abdominal wall and could thus prevent the identification of phase shifts. We expect that these effects are minor as we took precautions to suture the incision tightly and we clearly were able to measure EGGs after the laparotomy was performed. Nevertheless it is possible that uncoupling the electrical syncytium of the abdomen precludes the measurement of propagation in cutaneous electric signals. This question requires further study with multiple cutaneous electrodes.

Currently, biomagnetic measurements are performed inside a magnetically shielded room with equipment that operates with expensive cryogenics. Although these factors may limit the immediate clinical application of MGG, rapid advances are being made in superconductor technology and the ability to perform unshielded biomagnetic measurements is being perfected. Improvements in signal processing ability also encourage the application of SQUID technology to the sensitive measurements required for assessment of gastrointestinal electrical activity.

Our results suggest that multichannel MGG measurements can characterize healthy and uncoupled gastric tissue non-invasively and without making contact with the subject. The ability to routinely measure such clinical parameters as the gastric slow wave frequency and its propagation velocity could have significant impact in a clinical setting.

Acknowledgments

The authors wish to thank the personnel of the SR Light Laboratories at Vanderbilt Universities for their assistance with animal surgery. This work is supported in part by NIH Grants 1 R01 DK58197 and 1 R01 DK58697.

References

1. Hennig GW, Hirst GD, Park KJ, et al. Propagation of pacemaker activity in the guinea-pig antrum. J Physiol 2004;2:585–99. [PubMed: 14754999]
2. Stevens RJ, Weinert JS, Publicover NG. Visualization of origins, propagation of excitation in canine gastric smooth muscle. Am J Physiol 1999;1:C448–60. [PubMed: 10484332]

3. Simonian HP, Panganamamula K, Parkman HP, et al. Multichannel electrogastrography (EGG) in normal subjects: a multicenter study. Dig Dis Sci 2004;49:594–601. [PubMed: 15185863]
4. Zhang H, Xu X, Wang Z, Li C, Ke M. Correlation between gastric myoelectrical activity recorded by multi-channel electrogastrography and gastric emptying in patients with functional dyspepsia. Scand J Gastroenterol 2006;41:797–804. [PubMed: 16785192]
5. Levy J. Use of electrogastrography in children. Curr Gastroenterol Rep 2002;4:259–65. [PubMed: 12010628]
6. Mantides A, Stefanides G, Kioulanis J, Tzovaras G, Epanomeritakis E, Xynos E. Cutaneous electrogastrography for the assessment of gastric myoelectrical activity in type I diabetes mellitus. Am J Gastroenterol 1997;92:1190–3. [PubMed: 9219797]
7. Mintchev MP, Kingma YJ, Bowes KL. Accuracy of cutaneous recordings of gastric electrical activity. Gastroenterology 1993;104:1273–80. [PubMed: 8482441]
8. Familoni BO, Abell TL, Bowes KL. A model of gastric electrical activity in health and disease. IEEE Trans Biomed Eng 1995;42:647–57. [PubMed: 7622148]
9. Smout AJPM, van der Schee EJ, Grashuis JL. What is measured in electrogastrography? Dig Dis Sci 1980;25:179–87. [PubMed: 7371462]
10. Zhu H, Chen JD. Gastric distension alters frequency and regularity but not amplitude of the gastric slow wave. Neurogastroenterol Motil 2004;16:745–52. [PubMed: 15601424]
11. Chen J, McCallum RW. Response of the electric activity in the human stomach to water and a solid meal. Med Biol Eng Comput 1991;29:351–7. [PubMed: 1787749]
12. Lin Z, Chen JDZ, Schirmer BD, McCallum RW. Postprandial response of gastric slow waves: Correlation of serosal recordings with the electrogastrogram. Dig Dis Sci 2000;45:645–51. [PubMed: 10759228]
13. Geldof H, van der Schee EJ, van BM, Grashuis JL. Electrogastrographic study of gastric myoelectrical activity in patients with unexplained nausea and vomiting. Gut 1986;27:799–808. [PubMed: 3732889]
14. Camilleri M, Hasler WL, Parkman HP, Quigley EMM, Soffer E. Measurement of gastrointestinal motility in the GI laboratory. Gastro 1998;115:747–62.
15. Chen JD, Zou X, Lin X, Ouyang S, Liang J. Detection of gastric slow wave propagation from the cutaneous electrogastrogram. Am J Physiol 1999;1:G424–30. [PubMed: 10444457]
16. Krusiec-Swidergol B, Jonderko K. Multichannel electrogastrography under a magnifying glass–an in-depth study on reproducibility of fed state electrogastrograms. Neurogastroenterol Motil 2008;20:625–34. [PubMed: 18298438]
17. Mintchev MP, Otto SJ, Bowes KL. Electrogastrography can recognize gastric electrical uncoupling in dogs. Gastro 1997;112:2006–11.
18. Liang J, Chen JDZ. What can be measured from surface electrogastrography: computer simulations. Dig Dis Sci 1997;42:1331–43. [PubMed: 9246026]
19. Chang FY, Lee CT, Lee SD, Jang HC, Tsai DS, Fu SE. The influence of body size to the parameters of gastric slow wave: studied with an assembled electrogastrography. Chin J Physiol 1994;37:219–23. [PubMed: 7796638]
20. Bradshaw LA, Richards WO, Wikswo JP Jr. Volume conductor effects on the spatial resolution of magnetic fields and electric potentials from gastrointestinal electrical activity. Med Biol Eng Comput 2001;39:35–43. [PubMed: 11214271]
21. Won KJ, Sanders KM, Ward SM. Interstitial cells of Cajal mediate mechanosensitive responses in the stomach. Proc Natl Acad Sci USA 2005;102:14913–18. [PubMed: 16204383]
22. Allescher HD, Abraham-Fuchs K, Dunkel RE, Classen M. Biomagnetic 3-dimensional spatial and temporal characterization of electrical activity of human stomach. Dig Dis Sci 1998;43:683–93. [PubMed: 9558020]
23. Bradshaw LA, Ladipo JK, Staton DJ, Wikswo JP Jr, Richards WO. The human vector magnetogastrogram and magnetoenterogram. IEEE Trans Biomed Eng 1999;46:959–70. [PubMed: 10431461]
24. Bradshaw LA, Myers AG, Redmond A, Wikswo JP, Richards WO. Biomagnetic detection of gastric electrical activity in normal and vagotomized rabbits. Neurogastroenterol Motil 2003;15:475–82. [PubMed: 14507349]

25. Bradshaw LA, Irimia A, Sims JA, Gallucci MR, Palmer RL, Richards WO. Biomagnetic characterization of spatiotemporal parameters of the gastric slow wave. Neurogastroenterol Motil 2006;18:619–31. [PubMed: 16918726]
26. Turnbull GK, Ritcey SP, Stroink G, Brandts B, van Leeuwen P. Spatial, temporal variations in the magnetic fields produced by human gastroinestinal activity. Med Biol Eng Comput 1999;37:549–54. [PubMed: 10723890]
27. Richards WO, Bradshaw LA, Staton DJ, et al. Magnetoenterography (MENG): noninvasive measurement of bioelectric activity in human small intestine. Dig Dis Sci 1996;41:2293–301. [PubMed: 9011432]
28. Bradshaw, LA.; Wikswo, JP. Autoregressive, eigenfrequency spectral analysis of magnetoenterographic signals. Proc 17th Annu IEEE EMBS; 1995. CD-ROM
29. Bradshaw LA, Sims JA, Richards WO. Noninvasive assessment of the effects of glucagon on the gastric slow wave. Am J Physiol Gastrointest Liver Physiol 2007;293:G1029–38. [PubMed: 17884978]
30. Haberkorn W, Steinhoff U, Burghoff M, Kosch O, Morguet A, Koch H. Pseudo current density maps of electrophysiological heart, nerve or brain function and their physical basis. Biomagn Res Technol 2006;4:5. [PubMed: 17040559]
31. Irimia, A.; Gallucci, MR.; Richards, WO.; Bradshaw, LA. Separation of gastric electrical control activity from simultaneous MGG/EGG recordings using independent component analysis. Conf Proc IEEE Eng Med Biol Soc; 2006. p. 3110-3.
32. Staton, DJ.; Soteriou, MC.; Friedman, RN.; Richards, WO.; Wikswo, JP. First magnetic measurements of smooth muscle in vitro using a high-resolution. Proc 13th Annu Int; 1991. p. 550-1.
33. Irimia A, Richards WO, Bradshaw LA. Magnetogastrographic detection of gastric electrical response activity in humans. Phys Med Biol 2006;51:1347–60. [PubMed: 16481699]
34. Price CN, Westwick DT, Mintchev MP. Analysis of canine model of gastric electrical uncoupling using recurrence quantification analysis. Dig Dis Sci 2005;50:885–92. [PubMed: 15906764]
35. Irimia A, Wikswo JP Jr. Gastrointestinal arrhythmias are associated with statistically significant fluctuations in systemic information dimension. Physiol Meas 2008;29:N33–40. [PubMed: 18427160]
36. Irimia A, Bradshaw LA. Artifact reduction in magnetogastrography using fast independent component analysis. Physiol Meas 2005;26:1059–73. [PubMed: 16311453]
37. Lammers WJEP, Slack JR. Waves of slow, spike patches. News Physiol Sci 2001;16:138–44. [PubMed: 11443235]
38. Bauer AJ, Publicover NG, Sanders KM. Origin and spread of slow waves in canine gastric antral circular muscle. Am J Physiol 1985;1:G800–6. [PubMed: 4083358]
39. Mirizzi N, Stella R, Scafoglieri U. Model to simulate the gastric electrical control and the response activity. Med Biol Eng Comput 1986;24:157–63. [PubMed: 3754916]
40. Irimia A, Bradshaw LA. Ellipsoidal electrogastrographic forward modelling. Phys Med Biol 2005;50:4429–44. [PubMed: 16148402]

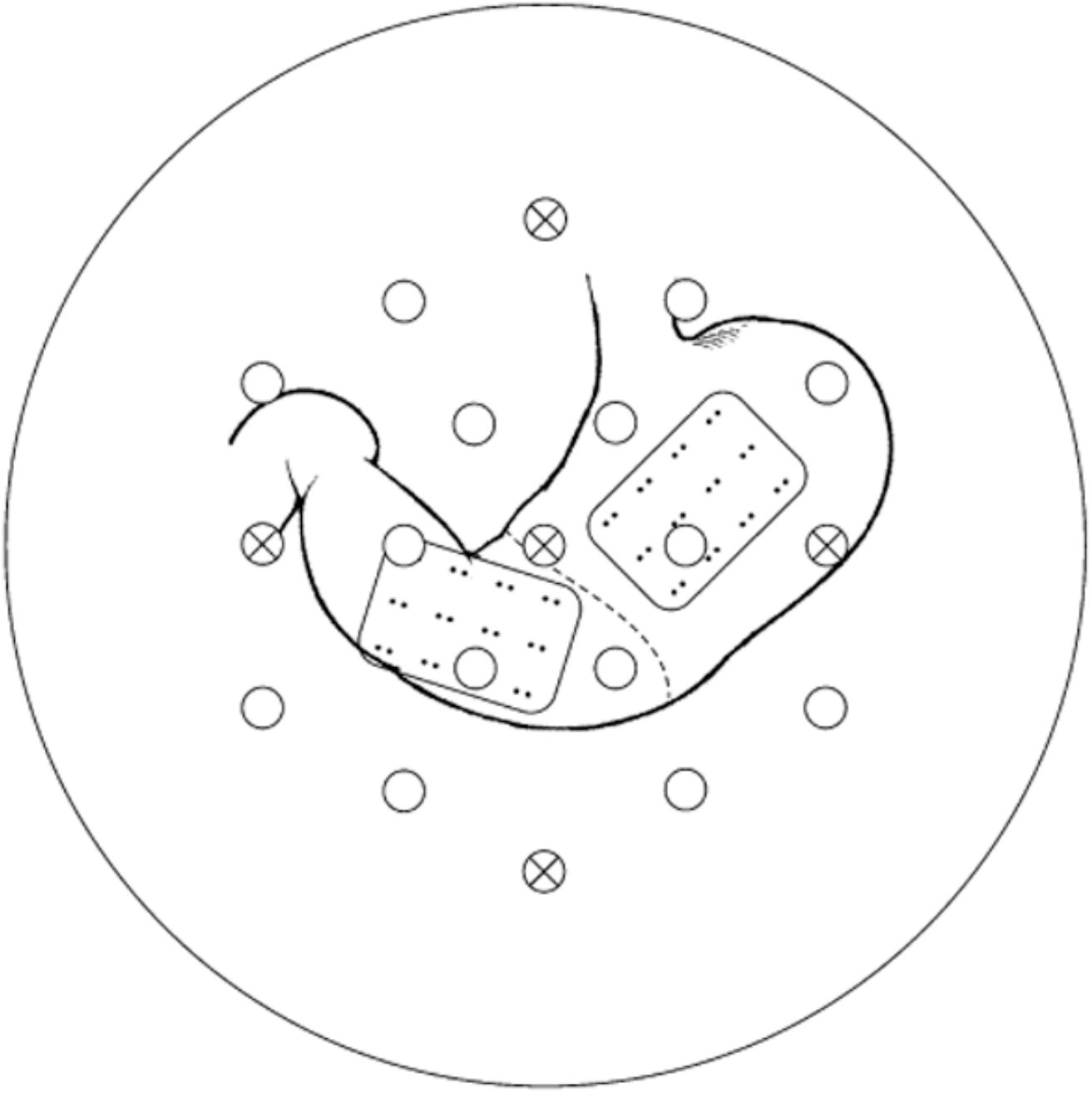

Figure 1.
Experimental setup illustrating approximate relative position of SQUID sensors and serosal electrodes. SQUID sensors are indicated by circles with vector sensors containing xs. Serosal electrode bipolar pairs have a baseline of 5 mm with a separation of 2 cm. The stomach was mechanically uncoupled by surgical division in the antrum at the approximate location of the indiciated dashed line.

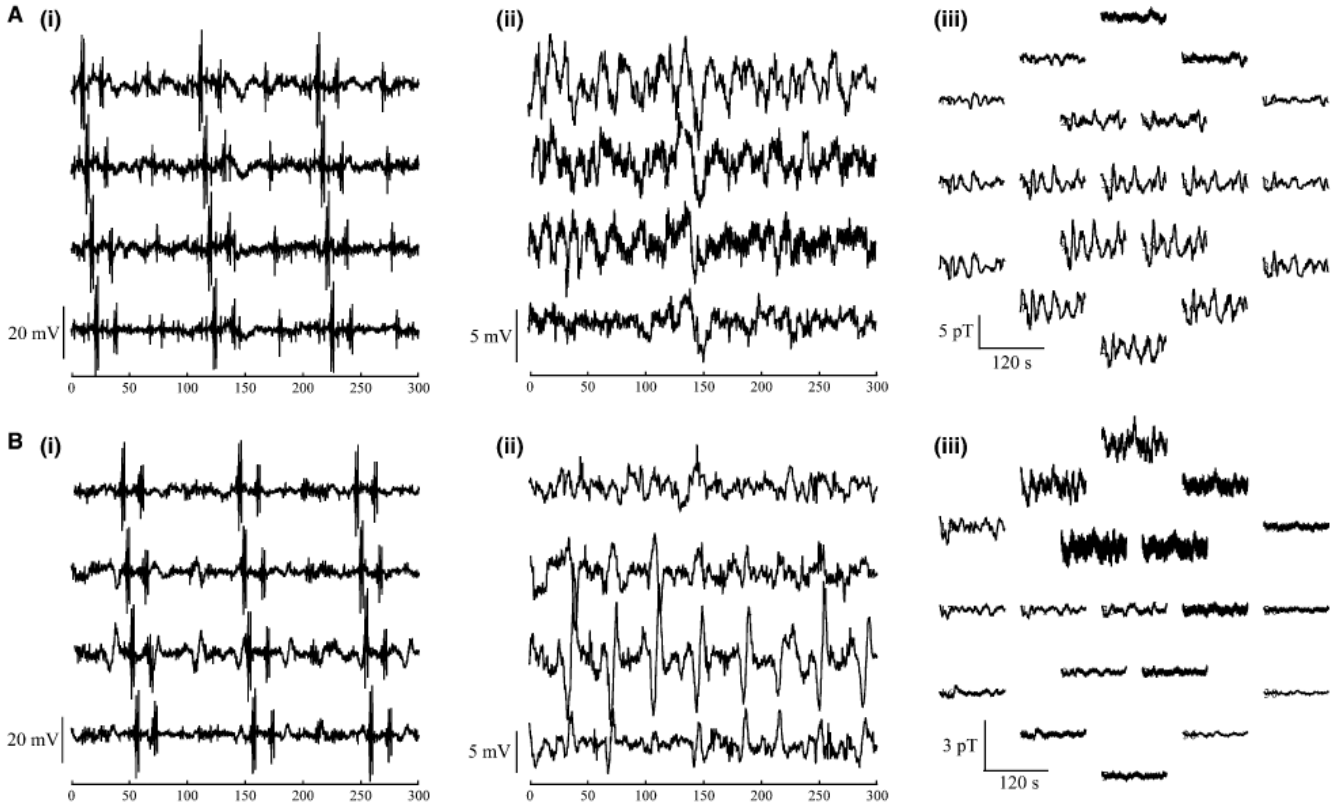

Figure 2.

Recordings (A) before and (B) after gastric division in (i) raw and (ii) filtered serosal electrodes and in (i) the multichannel SQUID magnetometer. Recordings from four sequential electrodes demonstrate propagation of spiking activity in unfiltered data (i). In panel (Aii) and (Bii) the spiking activity has been filtered to show only slow waves. Magnetogastrogram signals are mapped to the spatial location of the sensors (Aiii) before and (Biii) after gastric division.

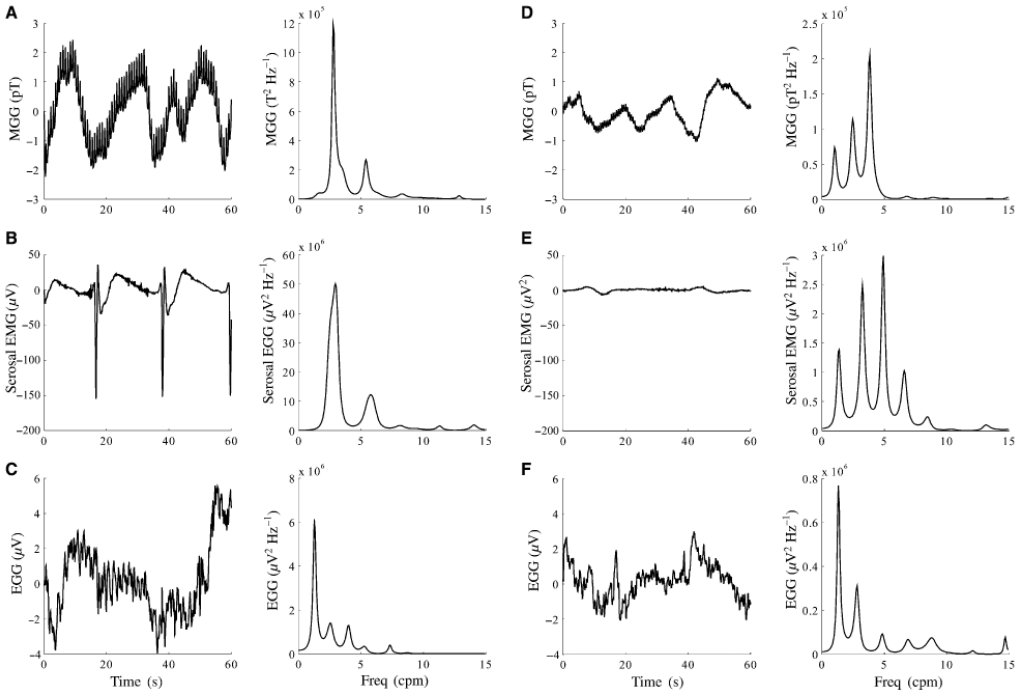

Figure 3.

Simultaneous MGG (A and D), serosal EMG (B and E) and EGG (C and F) signals and power spectra obtained during suspension of respiration before (A–C) and after (D–F) gastric division.

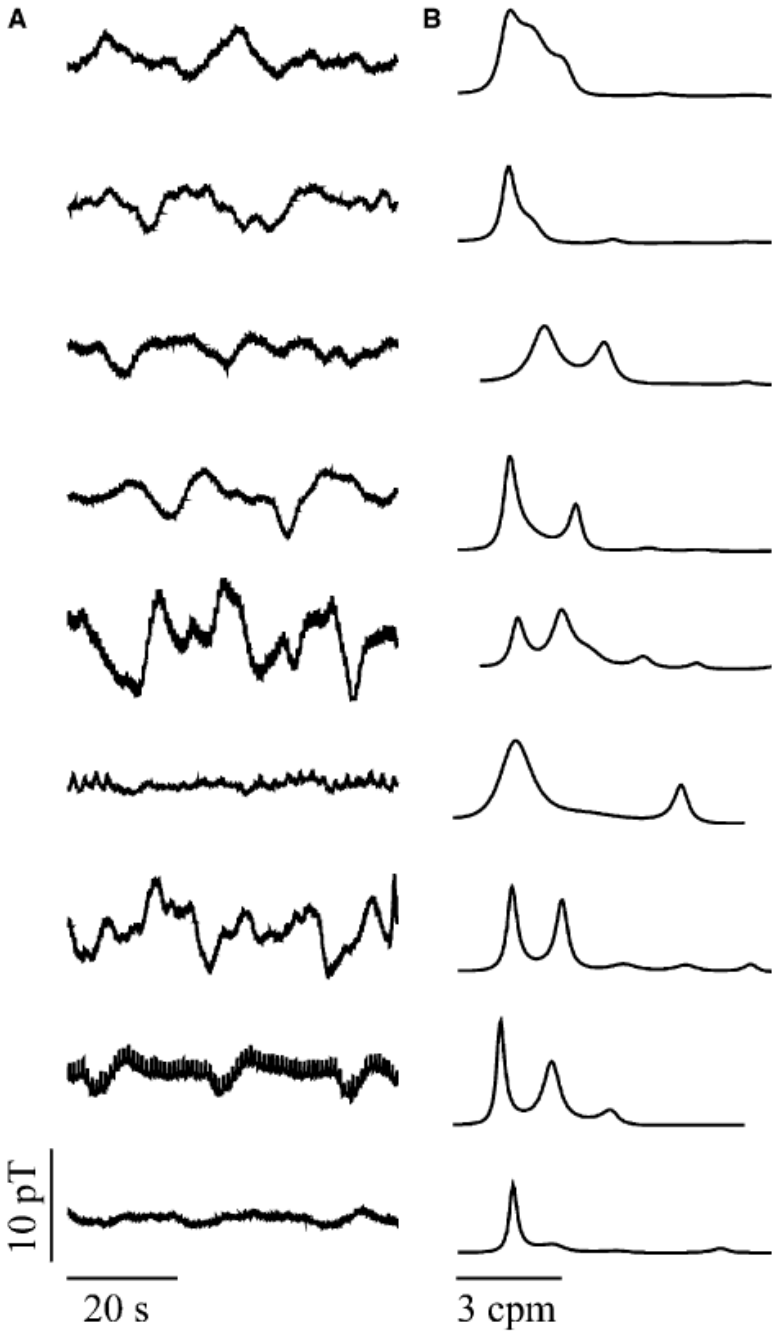

Figure 4.
Magnetogastrogram signals (A) and AR power spectra (B) recorded during baseline for each of the nine subjects. The dominant gastric slow wave frequency was identified from the power spectra.

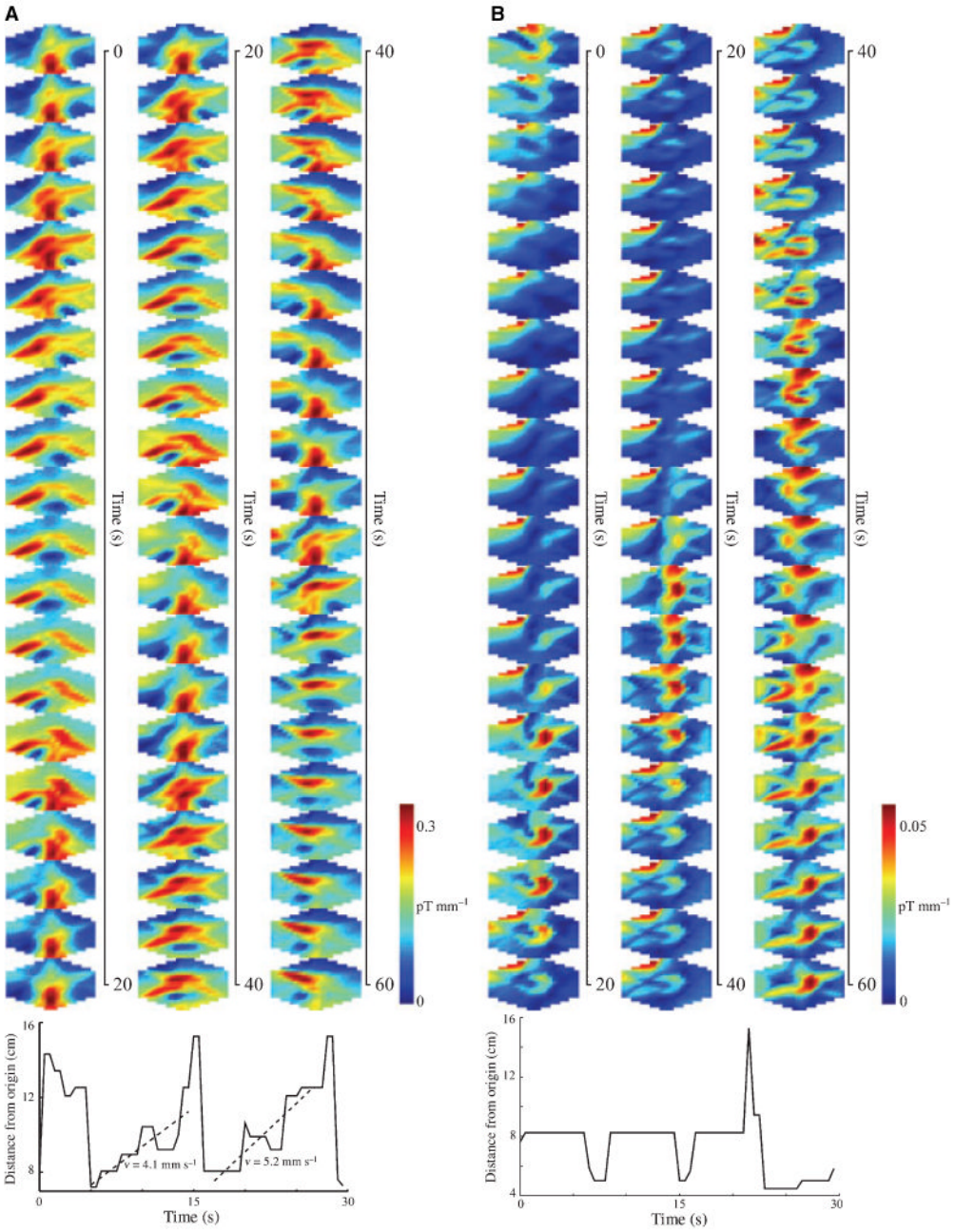

Figure 5.

Surface current density maps computed over 60 s of data. (A) Predivision SCD reveals a propagation pattern from the subject's left to right across the sensor array. The pattern repeats approximately every 15 s. (B) Postdivision, the pattern retains a periodicity of about 18 s, but the left-right propagation is not evident. The location of the SCD maxima as a function of time is shown below each set of SCD maps. Propagation velocity may be computed from these plots.

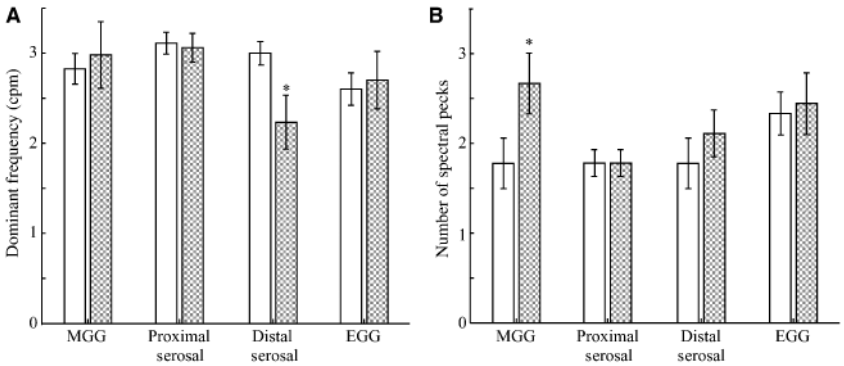

Figure 6.

(A) The average frequency and (B) the average number of spectral peaks from MGG, serosal EMG and EGG data before (solid) and after (shaded) gastric uncoupling. Although the distal serosal EMG recorded a significant decrease in postdivision dominant frequencies, no decrease was noted in MGG, EGG or the proximal serosal electrodes. However, there was a significant increase in the number of spectral peaks recorded postdivision in the MGG. This finding suggests that MGG records multiple frequencies present during uncoupling.

Table 1

Propagation velocities (mm s^{-1}) determined from four distal antral serosal electrodes and from the SCD estimate

	Predivision					Postdivision				
No. subjects	**V_1**	**V_2**	**V_3**	**V_4**	**SCD**	**V_1**	**V_2**	**V_3**	**V_4**	**SCD**
1	4.8	5.2	5.2	5.2	4.7	4.8	3.6	4.9	4.9	4.3
2	4.9	4.8	4.9	5.2	5.8	5.0	4.8	4.9	4.9	4.4
3	4.8	4.8	5.1	5.2	5.2	5.0	4.9	4.8	5.0	2.6
4	4.8	5.2	4.9	4.7	5.6	4.9	4.9	5.0	4.9	2.1
5	4.9	5.2	4.9	5.1	5.9	4.8	4.9	4.9	9.7	-11.0
6	5.1	5.1	4.9	5.1	5.1	4.9	5.0	3.7	7.5	5.3
7	4.9	4.9	5.1	4.6	4.6	5.0	4.9	3.3	11.0	4.3
8	4.9	5.1	4.7	6.1	5.4	5.0	4.9	4.7	5.3	-6.4
9	4.8	5.2	4.9	5.4	5.6	4.9	4.9	10.0	3.4	7.2
Mean	4.9	5.1	5.0	5.2	5.3	4.9	4.8	5.1	6.3	1.4
SD	0.1	0.2	0.1	0.4	0.5	0.1	0.5	1.9	2.6	6.0

SCD, surface current density.

Neurogastroenterol Motil. Author manuscript; available in PMC 2010 April 19.

Table 2

Percent power distributed (PPD) in brady-, normo- and tachygastric frequency ranges for (**a**) magnetogastrogram (MGG), (**b**) serosal electromyogram (EMG) and (**c**) electrogasrtogram (EGG)

	Brady-		Normo-		Tachy-	
No. subjects	**Pre**	**Post**	**Pre**	**Post**	**Pre**	**Post**
(a) MGG PPDs						
1	2.3	9.1	70.2	84.1	27.5	6.8
2	0.5	14.4	31.6	57.7	67.9	30.9
3	4.1	3.6	86.4	87.7	9.5	8.7
4	3.9	45.2	67.3	41.1	28.9	13.7
5	5.7	26.7	73.8	47.2	20.5	26.7
6	27.6	10.5	63.5	61.2	8.9	28.2
7	2.1	26.8	78.6	56.2	19.3	17.1
8	10.5	16.3	69.3	27.4	20.2	56.3
9	8.7	16.1	43.5	57.0	47.8	26.9
Mean ± SE	10.9 ± 3.8	25.2 ± 5.4*	52.1 ± 5.5	39.9 ± 5.7	37.0 ± 6.3	34.9 ± 5.6
(b) Serosal PPDs						
1	8.0	24.3	73.3	43.2	18.7	32.4
2	1.6	14.9	72.1	55.2	26.3	29.9
3	0.6	16.7	46.2	59.6	53.2	23.6
4	4.3	38.7	73.3	38.7	22.4	22.5
5	3.0	32.3	56.5	49.3	40.5	18.5
6	1.0	31.5	65.4	51.1	33.6	17.4
7	2.9	4.4	77.0	26.5	20.1	69.1
8	7.5	6.4	75.7	58.6	16.9	35.0
9	5.1	44.1	76.0	43.4	18.9	12.4
Mean ± SE	5.6 ± 1.3	31.2 ± 5.3*	59.3 ± 4.6	28.2 ± 2.6*	35.1 ± 5.4	40.6 ± 6.7
(c) EGG PPDs						
1	15.3	42.7	49.9	22.7	34.8	34.6
2	1.2	6.5	70.3	75.4	28.5	18.1
3	6.1	18.5	73.2	68.4	20.6	13.1

	Brady-		Normo-		Tachy-	
No. subjects	Pre	Post	Pre	Post	Pre	Post
4	2.9	5.1	49.4	56.9	47.7	38.0
5	22.0	4.9	44.8	79.4	33.2	15.8
6	6.4	31.2	44.9	42.6	48.7	26.1
7	7.6	12.0	65.2	31.8	27.2	56.2
8	28.5	19.3	61.3	74.9	10.1	5.8
9	2.7	9.9	86.0	66.1	11.3	24.0
Mean ± SE	15.9 ± 4.5	24.0 ± 5.0	50.7 ± 5.8	42.5 ± 6.3	33.5 ± 5.0	33.4 ± 5.9

* Indicates statistically significant differences.